SUPPORTING INFORMATION

Bismuth Silver Oxysulfide for Photoconversion Applications: Structural and Optoelectronic Properties

Amal BaQais,[a,b] Antton Curutchet,[c] Ahmed Ziani,[a] Hassan Ait Ahsaine,[a] Philippe Sautet,[d,e] Kazuhiro Takanabe,[a,*] Tangui Le Bahers[c,*]

[a]King Abdullah University of Science and Technology (KAUST), KAUST Catalysis Center (KCC) and Physical Sciences and Engineering Division (PSE), 4700 KAUST, Thuwal, 23955-6900, Saudi Arabia.

[b]Princess Nourah bint Abdulrahman University (PNU, College of Sciences, Department of Chemistry, Riyadh, 11671, Saudi Arabia.

[c]Univ Lyon, ENS de Lyon, CNRS, Université Claude Bernard Lyon 1, Laboratoire de Chimie UMR 5182, F-69342, Lyon, France.

[d]Department of Chemical and Biomolecular Engineering, University of California Los Angeles (UCLA), Los Angeles, CA 90095, United States.

[e]Department of Chemistry and Biochemistry, University of California Los Angeles, Los Angeles, CA 90095, United States

I. Rietveld analysis of BiAgOS.

Rietveld refinement was performed using the FullProf suite,[S1] which allows the refinement of atomic coordinates, site occupancies, atomic displacements and profile parameters (instrument parameters, background, lattice constants, full width at half maximum of the Bragg peaks and peak shapes). The PXRD profiles were fitted with the Thompson-Cox-Hastings pseudo-Voigt profile convoluted with axial divergence asymmetry. Figure S1 illustrates the plotted Rietveld refinements for the as-prepared BiAgOS sample.

The minimization was carried out using reliability index parameters such as the Bragg factors (R_{Bragg}), comparisons of the calculated and observed intensities (Y_{cal} and Y_{obs}), R_{wp} and the χ^2 factor. The final Rietveld cell parameters and the reliability factors are reported in Table S1. The obtained lattice constants are consistent with the DFT calculations.

Table S1. Rietveld-refined parameters of the BiAgOS structure.

Atoms	Wyckoff positions	x	y	z	B_{iso}	Occupancy
Bi	2c	¼	¼	0.137(5)	1.096(1)	1.0
Ag	2a	¾	¼	½	1.747(4)	1.0
S	2c	¼	¼	0.699(3)	1.649(6)	1.0
O	2a	¾	¼	0	0.919(3)	1.0
Reliability factors	R_{Bragg} = 8.7 %; R_{wp} = 8.05%; χ^2 = 2.7					
Cell parameters						
a / Å	b / Å	c / Å	V / Å^3	Space group	Density / g.cm^{-3}	
3.9137(1)	3.9137(1)	9.2279(2)	141.350(1)	P4/nmm	8.692	

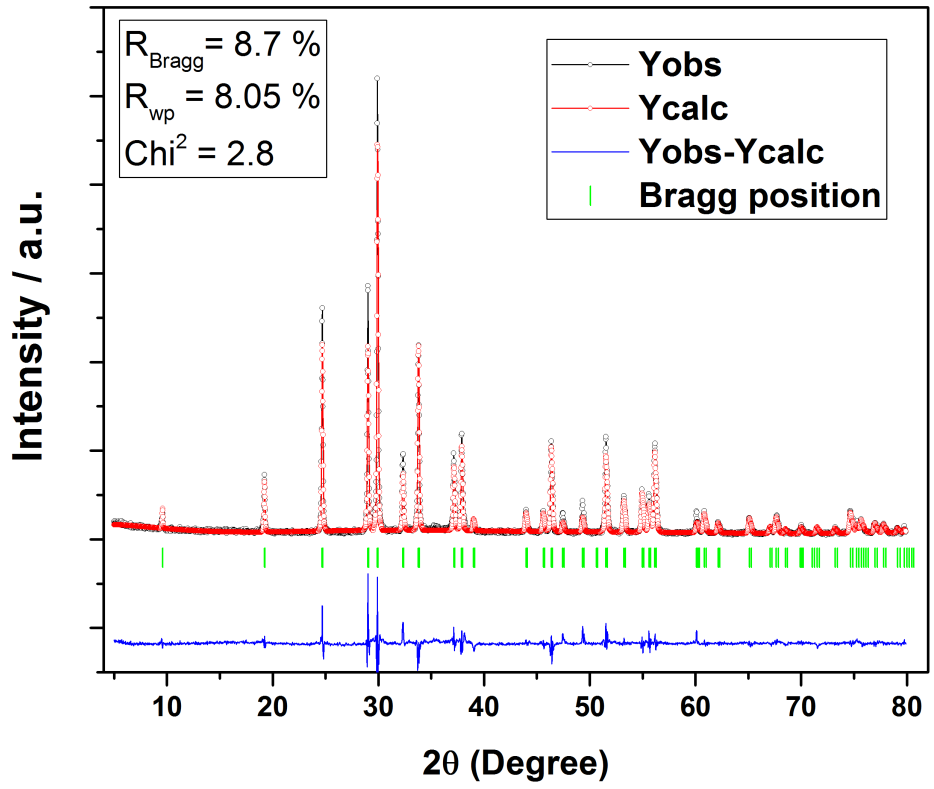

Figure S1. Rietveld-refined XRD spectrum of BiAgOS.

II. XPS and EDX analysis of BiCuOS.

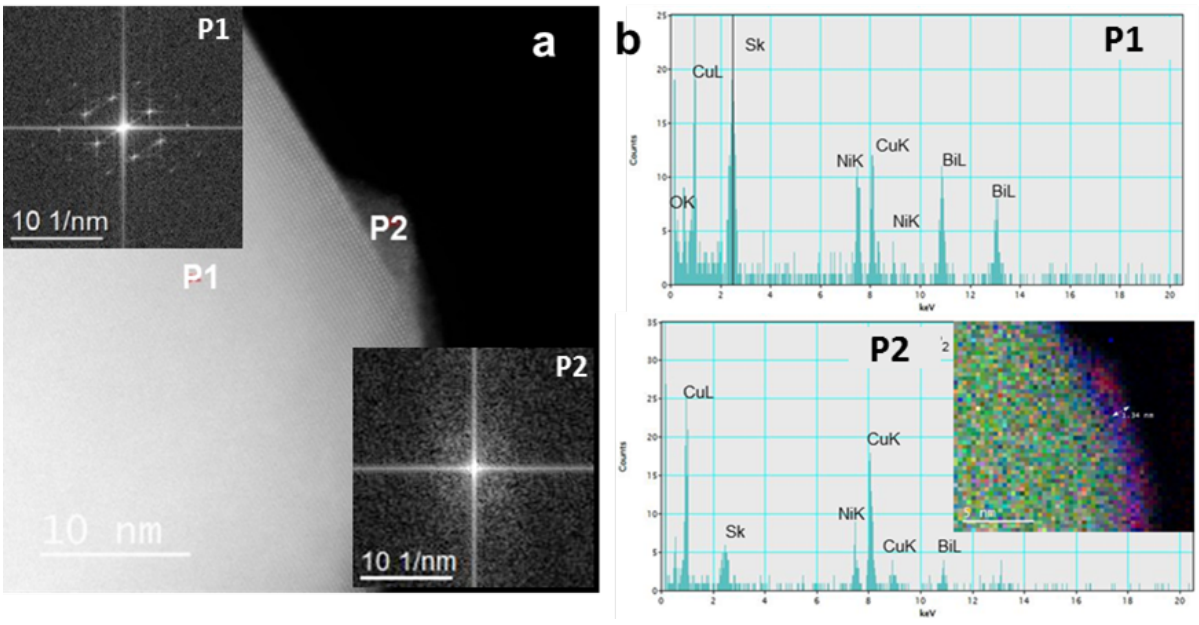

Figure S2. HR-TEM of the edge of BiCuOS (Inset FFT of different areas) (a), EDX spectra of different areas (inset mapping: Red-Cu, Green-S, Blue-O) (b).

III. Computed distances on the optimized PBE0 geometries.

Table S2. PBE0 computed bond lengths in Å.

	Bi-O	Bi-S	Cu/Ag-S
BiCuOS	2.314	3.143	2.426
BiAgOS	2.332	3.149	2.689

IV. Influence of the temperature on the particles morphology.

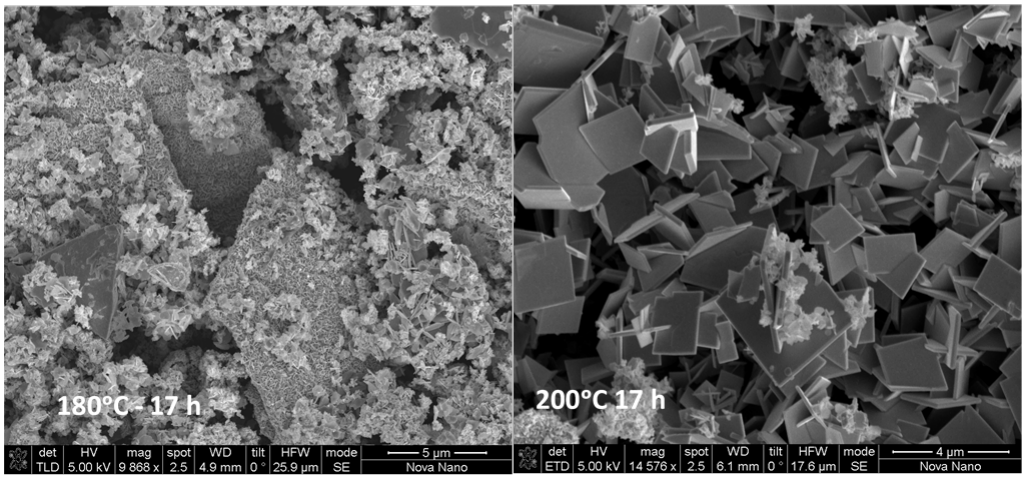

Figure S3: SEM images of BiCuOS synthesized at 180°C and 200°C during 17 h.

V. Large scan XPS spectra.

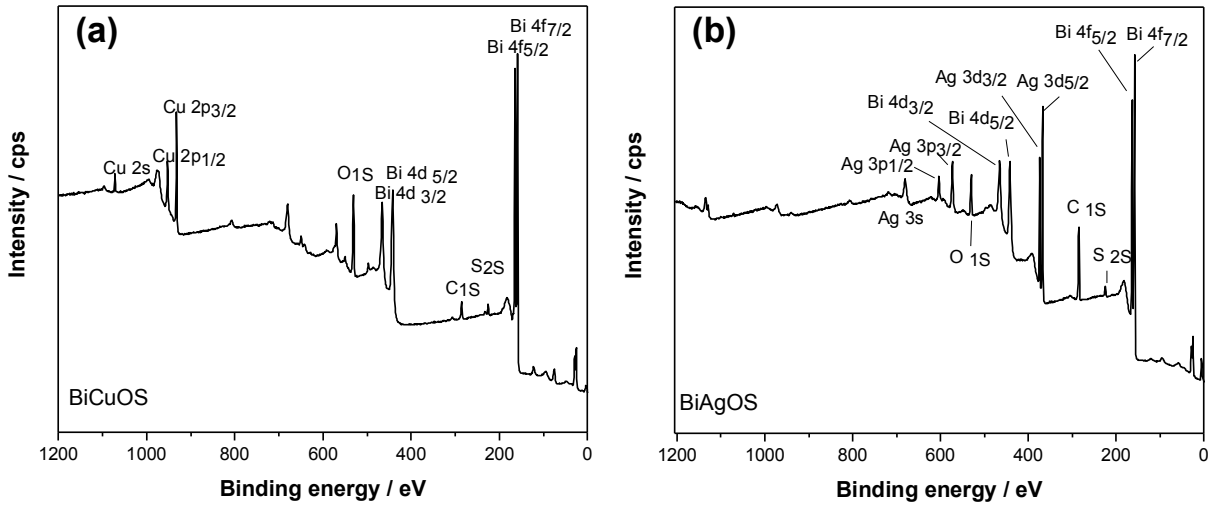

Figure S4. Wide scan XPS spectra of (a) BiCuOS and (b) BiAgOS.

VI. Influence of the cell parameters on the bandgap.

The influence of a and c cell parameters on the bandgap was estimated by varying these geometrical parameters by −5%, −2%, −1%, +1%, +2% and +5% from the experimental values. The results are presented in Figure S8. Interestingly, the a and c cell parameters variations have an opposite behavior on the bandgap. As expected, the a parameter (corresponding to the intra-layer direction) has a larger influence on the bandgap than the c parameter (inter-layer direction). A variation of 1% of the a parameter leads to variation of more than 0.1 eV on the bandgap.

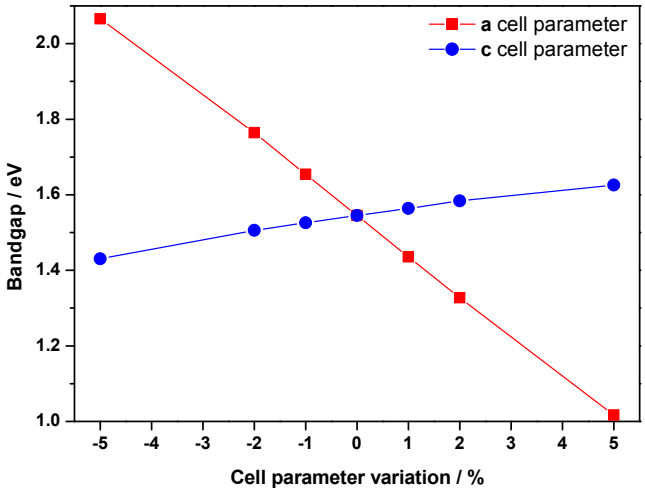

Figure S5. Influence of the cell parameters (presented as relative variation in %) on the bandgap of BiAgOS.

VII. Tauc plots to determine the indirect bandgaps.

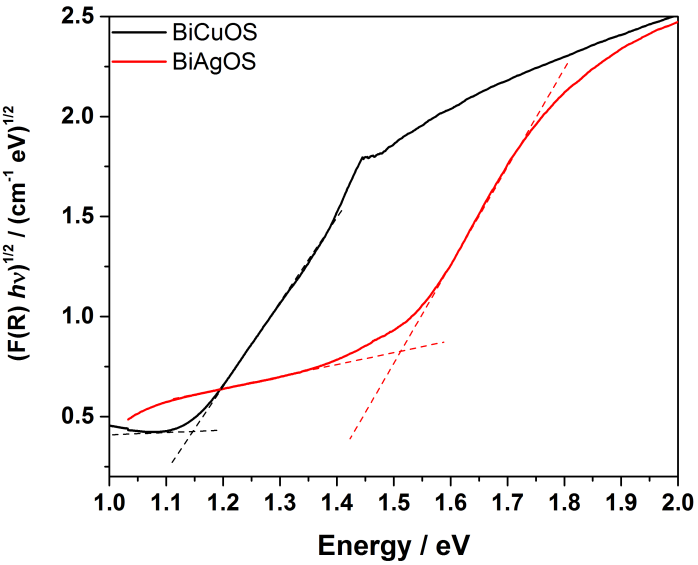

Figure S6. Associated Tauc plot used to determine the bandgaps for BiCuOS (black) and BiAgOS (Red). Dashed line interception was used for bandgap determination.

VIII. Thermogravimetric analysis.

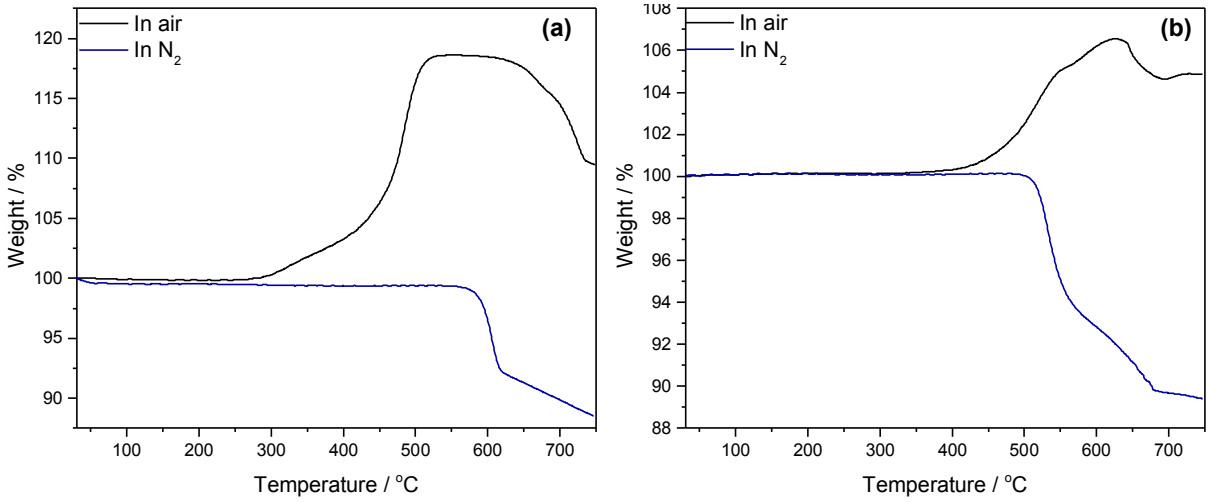

Figure S7. Thermogravimetric analysis of BiCuOS (a), BiAgOS (b) from room temperature to 750°C under flowing air (black curve) and N_2 (blue curve).

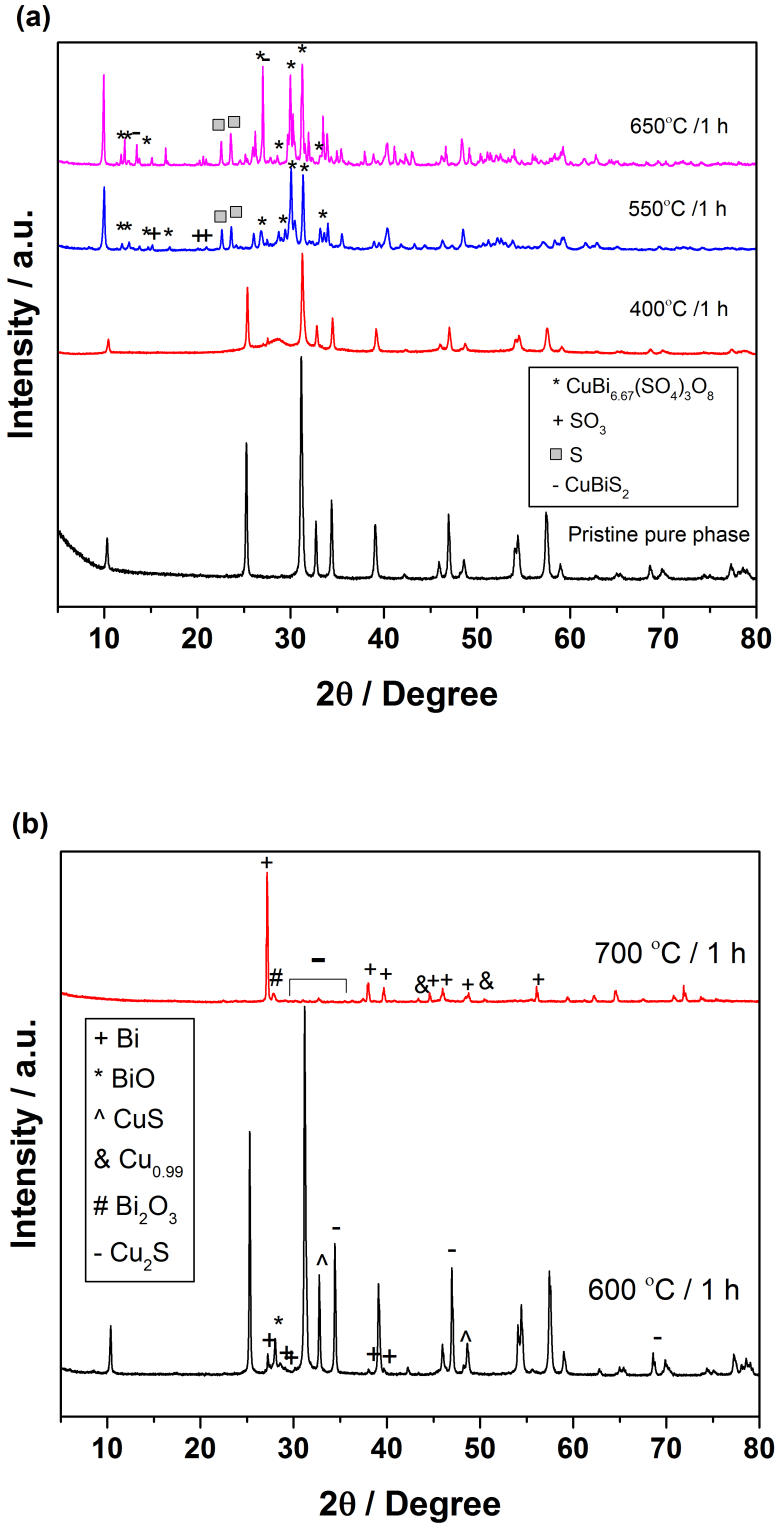

Figure S8. XRD pattern of BiCuOS (a) heated in air at different temperatures for 1 h or (b) heated in N_2 at different temperatures for 1 h.

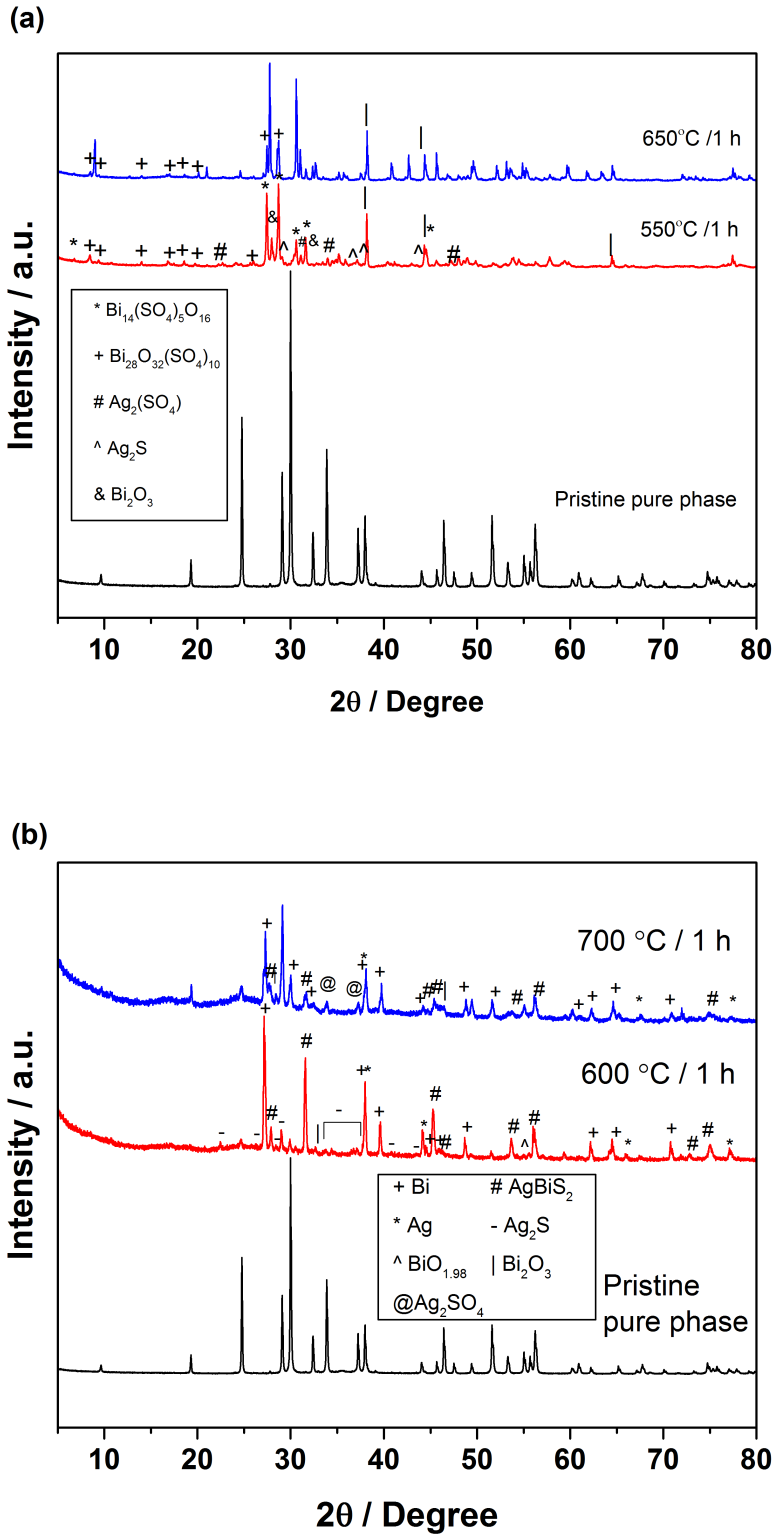

Figure S9. XRD pattern of BiAgOS (a) heated in air at different temperatures for 1 h or (b) heated in N_2 at different temperatures for 1 h.

IX. Calculation of the valence band effective density of states, Nv.

The valence band effective density of states, N_v, was calculated using the following formula derived from the free electron gas model using the hole effective mass (computed at the DFT level).

$$N_V = 2\left(\frac{2\pi m_h^* k_B T}{h^2}\right)^{3/2} \qquad \text{(S1)}$$

X. Influence of the pH on the flatband potential of BiCuOS.

The RHE reference electrode is a pH independent electrode correcting the NHE reference by the standard 0.06×pH term. Moving from Mott-Schottky plot drawn as a function of NHE (Figure S9 a) to a plot drawn as a function of RHE (Figure S10), for different pH, shows that the flatband potential of BiCuOS is pH independent.

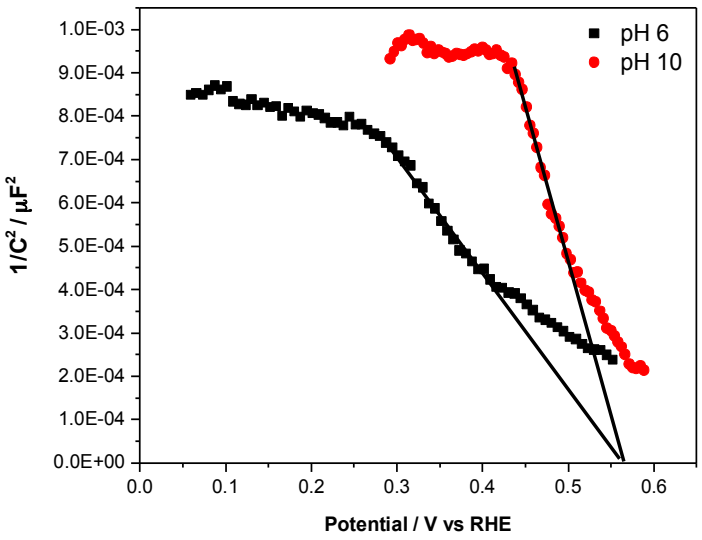

Figure S10: Mott-Schottky plots for BiCuOS pellets in 0.2 M Na_2SO_4 pH 6 (black) and pH 10 (red).

XI. Photocatalytic tests.

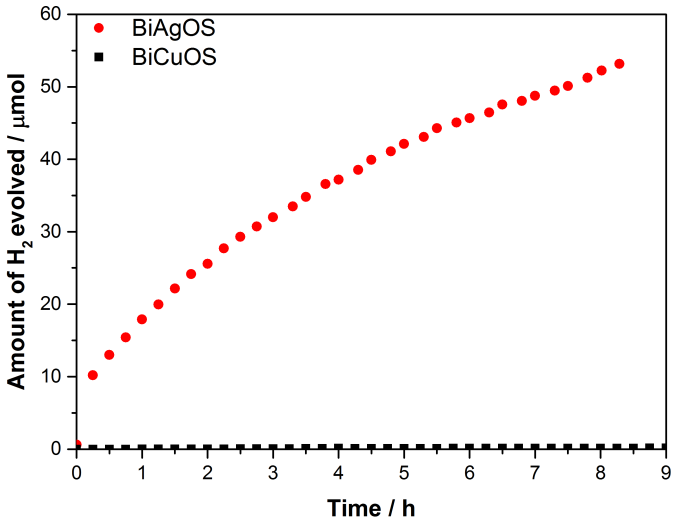

Figure S11. Photocatalytic time course of 1 wt% Ru/ BiCuOS and 1 wt% Ru/ BiAgOS (25 mL of 0.05 M Na_2S and 0.3 M Na_2SO_3 solution), the light irradiation (CM1 Cold mirror, 300 < λ < 800 nm), 50 mg of catalyst, and volume of reactor = 115 mL).

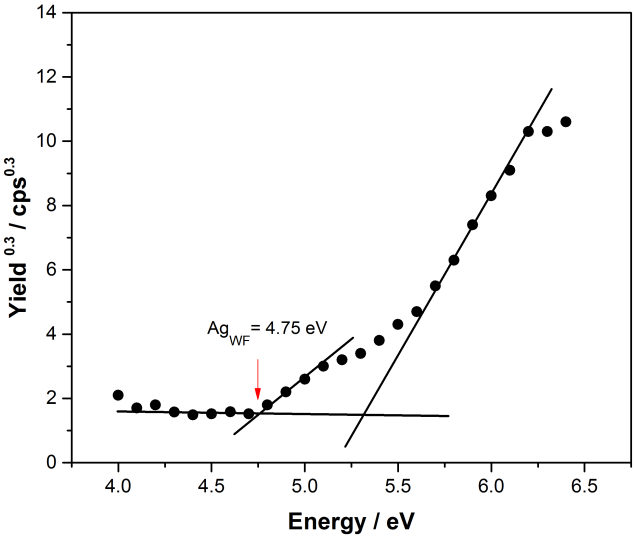

Figure S12. Photoelectron yield spectroscopy measurements of BiAgOS/ ITO electrodes in air after photocatalytic reaction.

References

(S1) Rodríguez-Carvajal, J. Recent Advances in Magnetic Structure Determination by Neutron Powder Diffraction. *Phys. B* **1993**, *192*, 55–69.